Journal of Applied Mathematics and Physics, 2022, 10, 1028-1035
https://www.scirp.org/journal/jamp
ISSN Online: 2327-4379
ISSN Print: 2327-4352

Morphology and Field Emission of ZnO Nanomaterials at Different Positions

Junzheng Wang, Lijun Wang

College of Science, University of Shanghai for Science and Technology, Shanghai, China
Email: wjunzheng00@163.com, wljpjchina@163.com

How to cite this paper: Wang, J.Z. and Wang, L.J. (2022) Morphology and Field Emission of ZnO Nanomaterials at Different Positions. *Journal of Applied Mathematics and Physics*, **10**, 1028-1035.
https://doi.org/10.4236/jamp.2022.104070

Received: March 3, 2022
Accepted: April 3, 2022
Published: April 6, 2022

Abstract

By simply adjusting the temperature and the number of materials, rod-like ZnO with different morphology, such as ZnO nanoneedles, were synthesized by a flexible thermal evaporation method. The ZnO nanorod array has the lowest turn-on field, the highest current density, and the highest emission efficiency due to its good contact with the substrate and relatively weak field shielding effect. Experiments show that the morphology and orientation of one-dimensional ZnO nanomaterials have a great influence on its conduction field and emission current density, and the nanoarrays also contribute to electron emission. The research results have a certain reference value for the application of ZnO nanorod arrays as cathode materials for field emission devices.

Keywords

Field Emission, ZnO Films, Vacuum Electron Beam Vapor Deposition

1. Introduction

Zinc oxide has a wide range of applications in sensors, actuators, solar cells, and biomedical samples, and has become one of the few dominant nanomaterials in the field of nanotechnology [1] [2] [3] [4] [5]. In recent years, ZnO has received increasing attention for its application in field emitters due to its low electron affinity, high aspect ratio, and oxidation resistance. Zinc oxide structures such as quadruped, nanowire, nanorods, nanowire and nanowire have field emission properties [6] [7] [8] [9]. These works confirm the potential application of ZnO in field emission (FE), but it is difficult to control the key factors affecting its FE performance. In general, electron emission is very sensitive to the shape of the emitter and the structure of the device. Therefore, it is necessary to study the effect of emitter morphology on its FE performance.

One-dimensional nanomaterials are the basic building blocks of nanostructured systems. One-dimensional nanomaterials have various morphologies, ranging from general shapes such as linear and rod structures to special shapes such as tubular structures. Its synthesis methods can be summarized into physical methods, chemical methods and physicochemical methods. More physical methods are used, such as laser deposition method, evaporation condensation method, etc. Common chemical methods include electrochemical preparation method, chemical vapor deposition method, liquid phase synthesis method, template method, common physical and chemical methods include evaporation suspension method, sol-gel-evaporation method. Vapor deposition method has become a widely used preparation method due to its simple growth process and high product quality. According to the different growth mechanisms of the gas phase method, it can be divided into the gas-liquid-solid method (VLS) and the gas-solid method (VS) [10] [11] [12].

In this work, a simple method, chemical vapor deposition, is introduced to synthesize ZnO nanostructures. Zinc oxides with different morphologies can be obtained by different positional relationships between the substrate and the reactants. The changes in the morphology of ZnO grown at different positions were investigated in detail. In addition, the FE properties of all prepared ZnO nanomaterials were systematically characterized and analyzed.

2. Experiments

In the preparation process of ZnO nanomaterials, first clean the substrate: ultrasonically clean the Si substrate with ethanol and deionized water for 10 minutes, repeat the cleaning of the Si substrate until it is clean, and there are no obvious crystal grains, and then blow it with a hair dryer. The dry-cleaned Si wafer is ready for use. Then prepare the copper film on the Si wafer: put the cleaned Si substrate into the sample tray of the vacuum coating machine, place the copper block (purity of 99.99%) in the electron beam crucible, turn on the vacuum pump system to pump the background pressure to 6.7×10^{-3} Pa (pressure maintenance needs to be low enough, at least as low as 7.0×10^{-3} Pa). Adjust the electron beam current, and at the same time observe the heating through the window, pay attention to adjusting the beam current not too fast, otherwise the copper block will splash instantly. During the period, the thickness of the copper film is monitored by the film thickness monitor. In order to control the influence of the catalyst, it is observed that the substrate surface is covered with a pale yellow film.

The Si substrate plated with copper film was placed in a tube furnace, heated to 900˚C for 20 minutes under nitrogen protection, and taken out for use after the temperature dropped to room temperature. To carry out the growth experiment of one-dimensional ZnO nanoarray structure, we prepared it on the basis of the CVD growth system. A gas flow meter was connected to the inlet end of the horizontal tube furnace to control the flow rate of the carrier gas; the other

end of the horizontal tube furnace was connected to vacuum system, combined with the installed vacuum pressure gauge, can adjust the reaction pressure in the furnace. In order to obtain the ZnO nanorod array structure with consistent orientation, and for the consideration of subsequent device preparation, based on the optimized growth conditions, we use Si as the substrate. A high-quality Cu thin film with a thickness of about 5 nm is deposited on the substrate. The specific preparation process of ZnO nanorod arrays by CVD method is as follows: First, weigh an appropriate amount of high-purity (99.99%) ZnO powder and graphite (99.97% purity) powder and mix them uniformly in an equimolar ratio of 1:1, place them at the bottom of a quartz boat, and then place them at a distance of 2 to 5 cm above the reactants. Put the Si substrate that has been cut into small pieces, and then translate the quartz boat into the horizontal tube furnace, and make the reactants at the bottom of the boat located in the heating center of the tube furnace. Close the tube furnace and turn on the mechanical pump to reduce the pressure in the furnace tube to a vacuum state (10 ~ 100 Pa). Open the inlet valve, and pass 100 sccm of N_2 into the furnace as a carrier gas. The reaction pressure was maintained at one atmosphere (Table 1).

According to a pre-set program, the temperature of the heating zone of the tube furnace was raised to the preset temperature at a heating rate of 10˚C per minute, and then kept at this temperature for one hour. After the one-hour growth process, the N_2 inlet valve was closed, and the system was cooled to room temperature naturally, and then the mechanical pump was turned off to take out the sample. In the process of preparing ZnO nanomaterials, the cavity is under negative pressure and high temperature, so there is no requirement for the temperature and humidity of the experimental environment.

3. Result and Discussion

3.1. Composition and Microstructure Characterization of Thin Film

In this paper, an XRD spectrometer was used to conduct XRD detection on the samples. Due to the high repeatability of the results obtained by the samples, only the most typical group was given. Figure 1 shows the XRD patterns of typical samples and the XRD diffraction of ZnO and Si peak standard card. The XRD patterns of the ZnO samples all show two significant diffraction peaks, which correspond to the (002) plane of ZnO. In addition, another characteristic

Table 1. Parameters employed for the ZnO.

Experimental process parameters	Values
Nitrogen gas flows/sccm	100
Total gas pressure/Pa	1.013×10^5
Location distance/cm	1 and 5
temperature/˚C	900
Plasma processing time/min	60

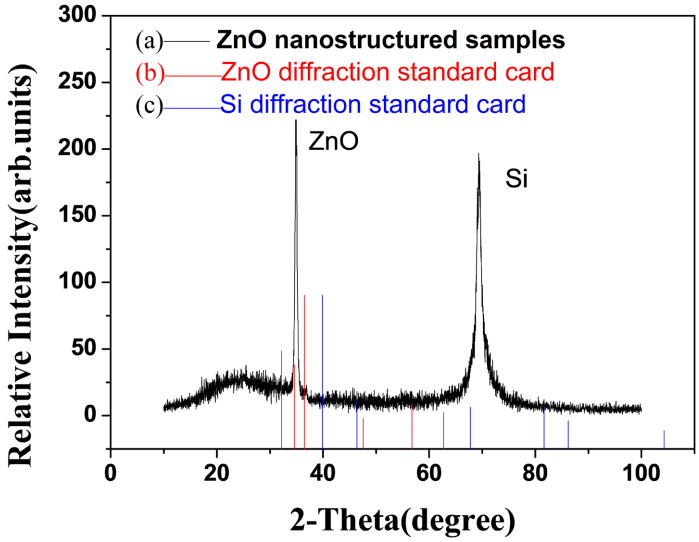

Figure 1. XRD spectrum of ZnO film. (a) A typical ZnO film sample; (b) Diffraction standard card of ZnO; (c) Diffraction standard card of Si.

diffraction peak belongs to the Si substrate. Except for these two peaks, no other peaks are found. Diffraction peaks, so this indicates that our prepared ZnO crystals have higher crystallinity and better quality.

3.2. Surface Morphology Characterization of ZnO Film

The VLS mechanism suggests that tiny alloy droplets can guide the growth of heterogeneous crystalline ZnO. The crystal VLS growth process can be divided into two steps: first, the catalyst and the reactants generate alloy droplets with a low eutectic temperature in a low temperature environment, that is, in a gas environment, the composition at the interface of the substrate has a strong effect on the reactant vapor. The gas phase-liquid phase transition layer with the capacity, which can continuously absorb the reactant vapor; in the next step, when the gas phase-liquid phase transition layer absorbs enough gaseous reactant molecules to be supersaturated, the transition layer in the liquid phase-solid phase transitions layer, that is, crystal nuclei are formed at the interface between the catalyst droplet and the substrate. With the continuous adsorption of the reactant vapor by the catalyst droplets, the reaction product will continue to precipitate from the liquid-solid phase transition layer, and the one-dimensional nanowire will continue to grow. The catalyst is insoluble in the reaction product, and the two exist independently. The catalyst will also be further and further away from the substrate. Therefore, the crystal VLS growth mechanism can be determined by the solid-state droplets left at the top of the nanowire.

The SEM images of the ZnO samples with different morphology synthesized under different conditions are shown in Figure 2. As shown in Figure 2(a), ZnO nanoblocks obtained at 900˚C were randomly stretched upward, and they were 100 nm. And the length is 2 μm. However, there are many scattered ZnO nanostructures in Figure 1(b), scattered on the substrate, each tooth is about 100 nm

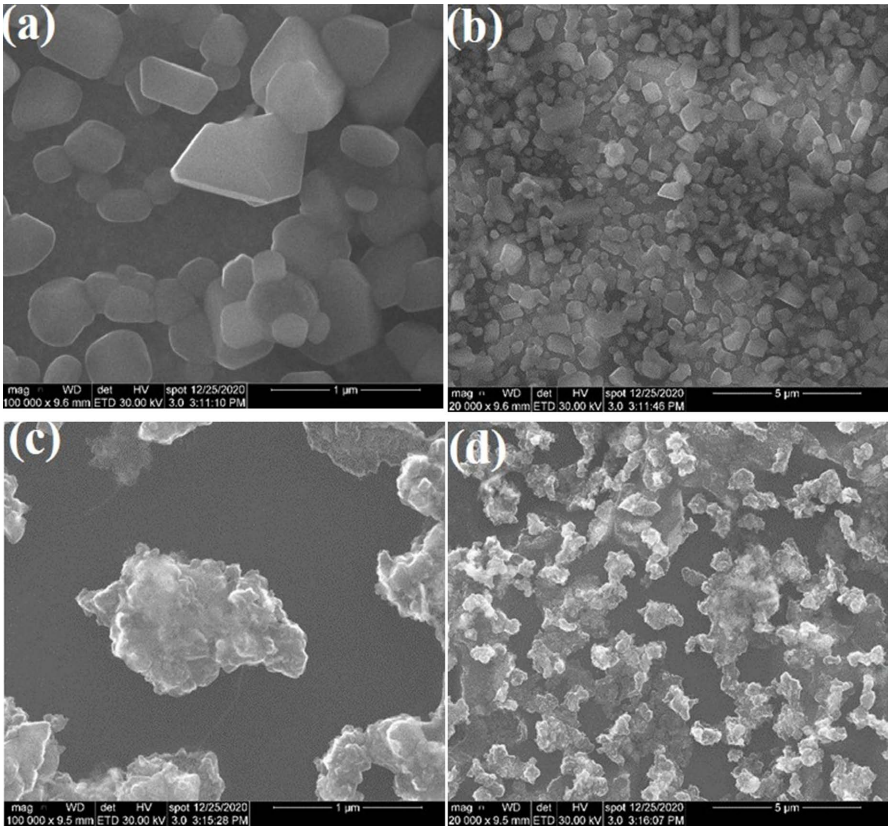

Figure 2. FE-SEM images of the surface of the ZnO film samples.

in diameter. Sample A (Figure 2(a)) and B (Figure 2(c)) are nanostacks. They are both of perfect size uniformity and perpendicular to the substrate. But sample A is denser and thinner than sample B.

The amount of Zn vapor adsorbed at different positions from the reactant is different. The alloy droplets close to the reactant receive the most Zn vapor. With the increase of the distance, the Zn content in the carrier gas decreases accordingly. The Zn vapor content adsorbed on the distant alloy droplets is correspondingly reduced. Therefore, the amount of the alloy droplets that can be adsorbed is also different, which affects the morphology of the ZnO nanostructures. The positions of the Si sheets at different positions have a gradient temperature, and the temperature is different between the farther and the nearer the reactant. When the temperature is high, the reactants of the ZnO nanostructure have enough energy to diffuse and move, and the Zn vapor with high energy may be decomposed and evaporated again, resulting in the inability of the ZnO nanostructure to grow stably. At cooler temperatures, the atoms don't have enough energy to deposit and form clusters where they land. Sample A is 1 cm from the material source, and sample B is 5 cm from the sample source. Therefore, compared with sample B, sample A had better structure and performance.

3.3. FE Performance of the ZnO Film

The iron properties of the ZnO thin film samples were tested. The results show

that the stability and reproducibility of various sample devices are good. Figure 3 shows the corresponding FE current density (J)-electric field (E) curves and Fowler-Nordheim (F-N) plots for ZnO thin film samples with different thicknesses. According to Figure 3, J increases exponentially with E. The threshold electric field (Eth) is defined as the electric field that produces J = 10 μA/cm^2. For ZnO thin film Sample A and Sample B, the corresponding FE Eth is 3.8 V/μm and 8.7 V/μm. Meanwhile, the corresponding maximum iron current densities are 354 μA/cm^2 and 340 μA/cm^2. It was found that the maximum emission current density of sample A was the best. However, it can also be seen from the curve that under the same external electric field, the current density of the ZnO thin film sample with a distance of 1 cm is not the maximum before being decomposed.

Our study provides ideas for the following researchers, who can try to improve the preparation process or crystal structure by physical or chemical methods to improve the FE of ZnO and broaden the way for the industrial application of ZnO. Compared with traditional physical coating preparation, CVD technology has the characteristics of better film quality and better ZnO purity. In industrial application, the low preparation cost and the large-scale preparation are not negligible advantages for ZnO. As shown in Figure 3, the F-N curves of all ZnO thin film samples show a certain negative slope linear relationship in the high electric field region (which is consistent with the traditional FE theory), but not in the low electric field region. This phenomenon is often observed in iron emitters with complex nanosurface topography, which should be attributed to the adsorption of some foreign gas on the surface of the emitter (the whole process from sample preparation to final placement into high vacuum FE equipment), it will inevitably come into contact with the atmosphere and will inevitably absorb some gases. Although some measures have been taken to reduce the effect of adsorbed gases, for example, samples should be kept in the laboratory before the FE test. For a period of time high vacuum environment in

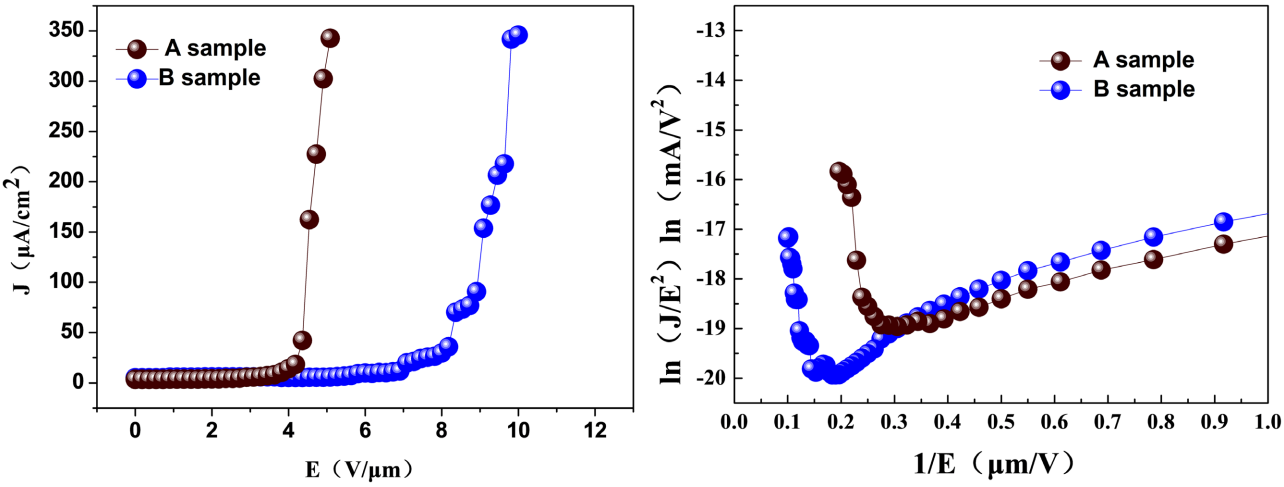

Figure 3. Field emission characteristic curves of ZnO film.

order to desorb as much gas as possible from the sample surface. However, even so, the effect of adsorbed gas on iron may not be completely eliminated. Under the action of a certain strength of the applied electric field, the adsorbed gas is ionized and discharged, so that the current detected in the iron experiment is mixed with the ionic current in addition to the electron current. Therefore, the emission characteristics at low electric fields do not conform to the traditional F-N theory. As the electric field increases, the gas is gradually ionized until the gas is adsorbed under the action of the electric field.

4. Conclusion

In summary, nanoneedle-type ZnO nanostructures were successfully synthesized by chemical vapor deposition. Experiments have shown that higher temperatures and enough oxygen help form more nuclei for further growth. The synthesis conditions largely affect the morphology of ZnO, especially the orientation and array. In addition, they also have a large impact on field emission capabilities. ZnO nanorod arrays have excellent field emission properties and are perpendicular to the substrate with appropriate spacing between adjacent nanorods. The prepared single-crystal oriented ZnO nanorods have potential applications in field emission and other optoelectronic devices.

Conflicts of Interest

The authors declare no conflicts of interest regarding the publication of this paper.

References

[1] Jiang, J., Pi, J. and Cai, J. (2018) The Advancing of Zinc Oxide Nanoparticles for Biomedical Applications. *Bioinorganic Chemistry and Applications*, **2018**, Article ID: 1062562. https://doi.org/10.1155/2018/1062562

[2] Chaudhary, S., Umar, A., Bhasin, K.K. and Baskoutas S. (2018) Chemical Sensing Applications of ZnO Nanomaterials. *Materials*, **11**, 287. https://doi.org/10.3390/ma11020287

[3] Sarmah, K. and Pratihar, S.S. (2017) Characterization and Photocatalytic Application of Iron Oxalate Capped Fe, Fe-Cu, FeCo, and Fe-Mn Oxide Nanomaterial. *ACS Sustainable Chemistry & Engineering*, **5**, 310-324. https://doi.org/10.1021/acssuschemeng.6b01673

[4] Das, P., Sarmah, K., Hussain, N., Pratihar, S., Das, S., Bhattacharyya, P., Patil, S.A., Kim, H.S., Iqbal, M., Khazie, A. and Bhattacharyya, S.S. (2016) Novel Synthesis of an Iron Oxalate Capped Iron Oxide Nanomaterial; A Unique Soil Conditioner and Slow-Release Eco-Friendly Source of Iron Sustenance in Plants. *RSC Advances*, **6**, 103012-25. https://doi.org/10.1039/C6RA18840K

[5] Alshamsi, H.A.H. and Hussein, B.S. (2018) Hydrothermal Preparation of Silver Doping Zinc Oxide Nanoparticles: Synthesis, Characterization and Photocatalytic Activities. Orient. *Journal of Chemistry*, **34**, 1898-1907. https://doi.org/10.13005/ojc/3404025

[6] Siddiqi, K.S., Rahman, A., Tajuddin and Husen, A. (2018) Properties of Zinc Oxide Nanoparticles and Their Activity against Microbes. *Nanoscale Research Letters*, **13**,

141. https://doi.org/10.1186/s11671-018-2532-3

[7] Tan, K.H., Lim, F.S., Toh, A.Z.Y., Zheng, X.X., Dee, C.F., Majlis, B.Y., Chai, S.P. and Chang, W.S. (2018) Tunable Spectrum Selectivity for Multiphoton Absorption with Enhanced Visible Light Trapping in ZnO Nanorods. *Small*, **14**, Article ID: 1704053. https://doi.org/10.1002/smll.201704053

[8] Jin, S.E. and Jin, H.E. (2019) Synthesis, Characterization, and Three-Dimensional Structure Generation of Zinc Oxide-Based Nanomedicine for Biomedical Applications. *Pharmaceutics*, **11**, 575. https://doi.org/10.3390/pharmaceutics11110575

[9] Son, D.Y., Bae, K.H., Kim, H.S. and Park, N.G. (2015) Effects of Seed Layer on Growth of ZnO Nanorod and Performance of Perovskite Solar Cell. *The Journal of Physical Chemistry C*, **119**, 10321-10328. https://doi.org/10.1021/acs.jpcc.5b03276

[10] Tang, M., Liu, Y., Liu, L., Lin, T. and Liu, X. (2021) Microstructure and Mechanical Properties of SiC/SiC Joints Reinforced by *In-Situ* Growth SiC Nanowires. *Materials Characterization*, **179**, Article ID: 111315. https://doi.org/10.1016/j.matchar.2021.111315

[11] Li, P., Wang, L., Sun, S., Tu, C. and Chen, C. (2021) The Growth Behaviors and High Controllability of GaN Nanostructures on Stripe-Patterned Sapphire Substrates. *Applied Surface Science*, **555**, Article ID: 149725. https://doi.org/10.1016/j.apsusc.2021.149725

[12] Eckert, J., Holzer, J.C., Krill, C.E. and Johnson, W.L. (1993) Mechanically Driven Alloying and Grain Size Changes in Nanocrystalline Fe-Cu Powders. *Journal of Applied Physics*, **73**, 2794-2802. https://doi.org/10.1063/1.353055